

---

# DIRECT MULTIPLE SHOOTING AND DIRECT COLLOCATION PERFORM SIMILARLY IN BIOMECHANICAL PREDICTIVE SIMULATIONS

---

A PREPRINT

 **P. Puchaud**

Laboratoire de Simulation et Modélisation du Mouvement  
École de kinésiologie et des Sciences de l'Activité Physique  
Université de Montréal, Laval, Canada  
Centre de réadaptation Marie-Enfant  
CHU Sainte-Justine, Montréal, Canada  
pierre.puchaud@umontreal.ca

 **F. Bailly**

INRIA, Univ Montpellier, Montpellier, France  
francois.bailly@inria.fr

 **M. Begon**

Laboratoire de Simulation et Modélisation du Mouvement  
École de kinésiologie et des Sciences de l'Activité Physique  
Université de Montréal, Laval, Canada  
Centre de réadaptation Marie-Enfant  
CHU Sainte-Justine, Montréal, Canada  
mickael.begon@umontreal.ca

February 17, 2023

## ABSTRACT

Direct multiple shooting (DMS) and direct collocation (DC) are two common transcription methods for solving optimal control problems (OCP) in biomechanics and robotics. They have rarely been compared in terms of solution and speed. Through five examples of predictive simulations solved using five transcription methods and 100 initial guesses in the Biotim software, we showed that not a single method outperformed systematically better. All methods converged to almost the same solution (cost, states, and controls) in all but one OCP, with several local minima being found in the latter. Nevertheless, DC based on fourth-order Legendre polynomials provided overall better results, especially in terms of dynamic consistency compared to DMS based on a fourth-order Runge-Kutta method. Furthermore, expressing the rigid-body constraints using inverse dynamics was usually faster than forward dynamics. DC with dynamics constraints based on inverse dynamics converged to better and less variable solutions. Consequently, we recommend starting with this transcription to solve OCPs but keep testing other methods.

**Keywords** transcriptions · mechanics · biomechanics · predictive simulation · optimization · human movement

## 1 Introduction

Predictive simulation based on the optimal control theory can be insightful in biomechanics and robotics. In both fields, rigid-multibody dynamics equations describe the physical behavior of the system. In robotics, optimal control is used in trajectory planning [Diehl et al., 2006]. In biomechanics, human motor behavior often incorporates elements of optimality, and optimal solutions can give us insight into how humans plan and carry out movements, as well as provide innovative techniques for solving complex tasks. It is worth noting that the models in biomechanics can rely on joint torque-driven models, as for robotics, or muscle-driven models. The latter adds an extra layer of dynamics

to optimal control programs (OCPs), leading typical musculoskeletal models to handle thousands of variables, and enlarging the OCPs [Febrer-Nafria et al., 2022]. Direct approaches are commonly used for transcribing OCPs related to rigid-body dynamics, as opposed to indirect approaches, which tend to be more challenging to implement and initialize [Kelly, 2017, Betts, 2010]. The most common transcription methods are direct single shooting, direct multiple shooting (DMS), and direct (DC) collocation. The superiority of one transcription over another is still a topic of ongoing debate. While DMS is more popular in robotics [Gifftaler et al., 2018, Sleiman et al., 2019], DC has gained popularity in biomechanics [Ezati et al., 2019, Febrer-Nafria et al., 2020, Lee and Umberger, 2016]. It is important to compare these transcriptions for the biomechanics community.

Direct single shooting has been used in biomechanics until recently [Geijtenbeek, 2019]. It has limitations, such as being susceptible to local minima and chaotic behavior due to its dependency on the initial solution. The direct single shooting approach inherits these ill-conditioned OCPs that are often not solvable numerically speaking and slow [Diehl et al., 2006]. DMS and DC approaches improve numerical stability and convergence time compared to direct single shooting [Betts, 2010]. DMS uses time-stepping numerical integration to simulate consecutive intervals of a trajectory, and the arrival node of intervals is constrained to be equal to the first node of the next interval [Bock and Plitt, 1984]. DMS transcription has proven its efficiency in solving various biomechanical problems, including tracking motions [Venne et al., 2022], predictive simulations such as acrobatic moves [Koschorreck and Mombaur, 2012, Charbonneau et al., 2020], gait [Felis and Mombaur, 2016], lifting techniques with an exoskeleton [Sreenivasa et al., 2017] and its optimal settings [Harant et al., 2017, Sreenivasa et al., 2018]. In DC, the system states are approximated with polynomial splines on a temporal grid, and optimization ensures that the splines obey the system’s dynamics at collocation points [Biegler, 1984]. Direct collocation has been used for different biomechanics-related problems such as tracking motions [Lin and Pandy, 2017], and gait predictive simulations [Ackermann and van den Bogert, 2010, Miller and Hamill, 2015, Falisse et al., 2022]. However, both DMS and DC approaches have been applied to solve biomechanical problems, but no study has provided a fair comparison of these transcriptions.

DMS and DC transcriptions are not that different when looking at their transcriptions (see Sec. 2.1). Indeed, when using a DMS approach with an implicit Runge-Kutta (IRK) solver, the splines obey the system’s dynamics at collocation points through a Newton descent in the IRK solver. When using direct collocation, the same splines obey the dynamics through the constraints of the non-linear program (NLP) solver. The implicit formulations used to build the rigid-body dynamic constraints ( $F(\mathbf{x}, \dot{\mathbf{x}}, \mathbf{u}) = 0$ ) affects the results [Ferrolho et al., 2021]. Researchers have reported key methodological advances, including efficiently handling rigid-body and muscle dynamics through implicit formulations [Van Den Bogert et al., 2011, De Groote et al., 2016, Puchaud et al., 2023], which have been recommended to solve OCPs in biomechanics. For instance, Docquier et al. [2019] showed that direct collocations OCPs reached lower optima when rigid-body dynamic constraints matched joint acceleration through forward dynamics ( $\ddot{\mathbf{q}} - FD(\mathbf{q}, \dot{\mathbf{q}}, \boldsymbol{\tau}) = 0$ ) and that the CPU time was lower matching joint torques through inverse dynamics ( $\boldsymbol{\tau} - ID(\mathbf{q}, \dot{\mathbf{q}}, \ddot{\mathbf{q}}) = 0$ ). In an effort to include as many formulations as possible, the present study will assess the performance between these transcriptions (DMS with explicit RK, DMS with IRK, DC) and the formulation of rigid-body dynamic constraints.

Evaluating the optimality of OCPs commonly involves sensitivity studies with initial guesses. OCP have either been started with data-informed initial guesses close to an expected solution [Falisse et al., 2019] or with noise [Charbonneau et al., 2022]. For the present study, multi-start approaches with random noise were chosen because they are more challenging as they test the ability of OCPs to converge toward the same optimum [Puchaud et al., 2023]. Such approaches are needed to compare different transcriptions between them in terms of optimality. Recently, more and more direct transcriptions rely on fixed-step ordinary differential equations (ODE) integrators, favored by algorithmic differentiation [Andersson et al., 2019]. Unfortunately, the integration errors cannot be controlled anymore by the integrators while solving an OCP by using adaptive step size ODE solvers [Serban and Hindmash, 2008] or adaptive mesh refinement [Patterson and Rao, 2014]. Thus, there is a need for metrics to assess the dynamic consistency of the optimal solutions found. While this step is essential to evaluate the dynamics consistency of the solution, this practice has not been frequently done when using direct collocation [Michaud et al., 2022]. The dynamics consistency of direct transcriptions must be examined to estimate the reliability of all optimal solutions found with multi-start approaches.

This study aims to evaluate the performance of various direct optimal control transcriptions and dynamic formulations on five OCPs. First, we will review how the optimal control problem is transcribed from the continuous optimal control problem into non-linear programming through DC and DMS transcriptions. Second, we will present two ways of formulating rigid-body constraints through forward or inverse dynamics. Then, five problems of increasing complexity will be presented to benchmark these transcriptions. To evaluate the performance of each transcription, the convergence rates, the CPU time to converge, optimality, and dynamic consistency of solutions will be evaluated in a multi-start scheme.

## 2 Background

This section will present the transcription of continuous trajectory optimization problems (2.1) into direct collocation (2.2) and direct multiple shooting (2.3). Finally, the dynamics constraints specific to rigid-body dynamics will be described (2.4).

### 2.1 Trajectory optimization

Let's consider any system whose dynamics is governed by an ODE of the form  $\dot{\mathbf{x}} = \mathbf{f}(\mathbf{x}, \mathbf{u})$ , with  $\mathbf{x}$  the state vector of size  $n_x$  and  $\mathbf{u}$  the control vector of size  $n_u$ . A generic trajectory optimization problem can be written as:

$$\min_{\mathbf{x}(\cdot), \mathbf{u}(\cdot)} \quad \phi(\mathbf{x}(t), \mathbf{u}(t)) \quad (1a)$$

$$\text{s.t.} \quad \mathbf{x}(0) - \mathbf{s}_0 = 0, \quad \text{Initial state constraint} \quad (1b)$$

$$\forall t \in [0, T], \quad \dot{\mathbf{x}}(t) - \mathbf{f}(\mathbf{x}(t), \mathbf{u}(t)) = 0, \quad \text{Dynamics constraints} \quad (1c)$$

$$\forall t \in [0, T], \quad \mathbf{g}(\mathbf{x}(t), \mathbf{u}(t)) \leq 0, \quad \text{Path constraints} \quad (1d)$$

$$\mathbf{r}(\mathbf{x}(T)) \leq 0, \quad \text{Terminal constraint} \quad (1e)$$

with  $\mathbf{s}_0$  the initial state and  $T$  the final time of the problem. The cost function is denoted  $\phi$ . The inequality constraints are gathered in a function  $\mathbf{g}$ , and the terminal constraint is represented by  $\mathbf{r}$ . This continuous-time optimization problem must be transcribed into a finite-dimensional nonlinear program (NLP) to be numerically tractable. To discretize this problem, two transcription approaches are described in the following: *direct collocation*, and *direct multiple shooting*. The main differences between them are the way they handle the simulation and optimization. DC does both simultaneously, whereas DMS first simulates and then, optimizes the trajectories.

### 2.2 Direct collocation transcription

In direct collocation, the control trajectory  $\mathbf{u}(t)$  is discretized into a finite-dimension vector  $\mathbf{u} = [\mathbf{u}_0 \dots \mathbf{u}_n \dots \mathbf{u}_{N-1}]$  of size  $N$ , at times  $t_n$ , called knot points with  $n \in [0..N-1]$ . The state trajectory  $\mathbf{x}(t)$  is similarly discretized with  $\mathbf{x} = [\mathbf{x}_0 \dots \mathbf{x}_n \dots \mathbf{x}_N]$  of size  $N+1$ , at times  $t_n$ , with  $n \in [0..N]$ .  $M$  collocation points subdivide the intervals  $[t_n, t_{n+1}]$  at times  $t_{n,m}$ , with  $m \in [0..M-1]$ . At these collocation points, intermediate states are denoted by  $\mathbf{x}_{n,m}$ . For the sake of compactness, at each knot points we introduce a vector of intermediate states  $\tilde{\mathbf{x}}_n = [\mathbf{x}_{n,0}, \dots, \mathbf{x}_{n,M-1}]$ . The main idea behind collocation transcriptions is to model the state trajectory  $\mathbf{x}(t)$  by a set of  $N$  polynomials  $\mathbf{p}_n$ , parametrized by the intermediate states  $\mathbf{x}_{n,m}$ . In the present work, we will focus on the specific case of *orthogonal collocations*, where the polynomials are Lagrange ones, such that:

$$\forall t \in [t_n, t_{n+1}], \quad \mathbf{p}_n(t, \tilde{\mathbf{x}}_n) = \sum_{m=0}^M \mathbf{x}_{n,m} \ell_{n,m}(t) \in \mathbb{R}^{n_x}, \quad (2)$$

$$\ell_{n,m}(t) = \prod_{k=0, k \neq m}^M \frac{t - t_{n,k}}{t_{n,m} - t_{n,k}} \in \mathbb{R}.$$

Properties of Lagrange polynomials entail that  $\mathbf{p}_n(t_{n,m}, \tilde{\mathbf{x}}_n) = \mathbf{x}_{n,m}$ . Then, the dynamics constraints (Eq. 1c) are satisfied at every collocation point:

$$\forall (n, m) \in [0..N-1] \times [0..M-1], \quad \mathbf{f}(\mathbf{p}_n(t_{n,m}, \tilde{\mathbf{x}}_n), \mathbf{u}_n) = \dot{\mathbf{p}}_n(t_{n,m}, \tilde{\mathbf{x}}_n). \quad (3)$$

These collocation conditions are included in the NLP, yielding a large-scale but sparse problem, which can be written as:

$$\min_{\tilde{\mathbf{x}}, \mathbf{u}} \quad \phi(\tilde{\mathbf{x}}, \mathbf{u}) \quad (4a)$$

$$\text{s.t.} \quad \mathbf{x}_{0,0} - \mathbf{s}_0 = 0, \quad (4b)$$

$$\forall (n, m) \in [0..N-1] \times [0..M-1], \quad \mathbf{f}(\mathbf{p}_n(t_{n,m}, \tilde{\mathbf{x}}_n), \mathbf{u}_n) = \dot{\mathbf{p}}_n(t_{n,m}, \tilde{\mathbf{x}}_n), \quad (4c)$$

$$\forall n \in [0..N-1], \quad \mathbf{p}_n(t_{n+1}, \tilde{\mathbf{x}}_n) - \mathbf{x}_{n+1,0} = 0, \quad (4d)$$

$$\forall n \in [0..N-1], \quad \mathbf{g}(\mathbf{x}_n, \mathbf{u}_n) \leq 0, \quad (4e)$$

$$\mathbf{r}(\mathbf{x}_N) \leq 0. \quad (4f)$$

One may note that the optimization variable  $\tilde{\mathbf{x}}$  directly corresponds to the coefficients of the Lagrange polynomials. Continuity constraints on  $p_n$  (Eq. 4d) ensure state continuity between the end of one interval and the beginning of the next one.

### 2.3 Direct multiple shooting transcription

We introduce the discretized control trajectory  $\mathbf{u} = [\mathbf{u}_0 \dots \mathbf{u}_n \dots \mathbf{u}_{N-1}]$  of size  $N$  and the discretized state trajectory  $\mathbf{x} = [\mathbf{x}_0 \dots \mathbf{x}_n \dots \mathbf{x}_N]$  of size  $N + 1$ . In DMS, the system ODE (Eq. 1c), is numerically solved on each interval as an initial value problem. State continuity constraints entail that the end of one interval coincides with the beginning of the next, to ensure the continuity of the trajectory, leading to the following NLP:

$$\min_{\mathbf{x}, \mathbf{u}} \quad \phi(\mathbf{x}, \mathbf{u}) \quad (5a)$$

$$\text{s.t.} \quad \mathbf{x}_{0,0} - \mathbf{s}_0 = 0, \quad (5b)$$

$$\forall n \in [0..N - 1], \quad \mathbf{x}_{n+1} = \mathbf{x}_n + \int_{t_n}^{t_{n+1}} \mathbf{f}(\mathbf{x}_n, \mathbf{u}_n) dt, \quad (5c)$$

$$\forall n \in [0..N - 1], \quad \mathbf{g}(\mathbf{x}_n, \mathbf{u}_n) \leq 0, \quad (5d)$$

$$\mathbf{r}(\mathbf{x}_N) \leq 0, \quad (5e)$$

The flexibility of DMS comes from the choice of the ODE solver needed to compute the continuity constraint (Eq. 5c), which ensures the consistency of the dynamics, for example:

- explicit Runge-Kutta (ERK) integrators (*e.g.*, 2nd order, 4th order), which are fast and precise enough for most applications;
- collocation-based IRK; interestingly, the collocation conditions of the DC transcription (Eq. 3) are mathematically equivalent to a DMS formulation with an implicit Runge-Kutta ODE solver [Wright, 1970, Série et al., 1969, Hairer et al., 2006]. Numerically, the DMS transcription with IRK ensures the constraints through a Newton-Raphson descent, while, in DC, they are solved directly in the optimizer;
- variable-step and order-step integrators, such as RK45 or CVODES [Serban and Hindmarsh, 2008], make this transcription method theoretically as precise as desired regarding the dynamical consistency of the solutions, thanks to the adaptive step size control.

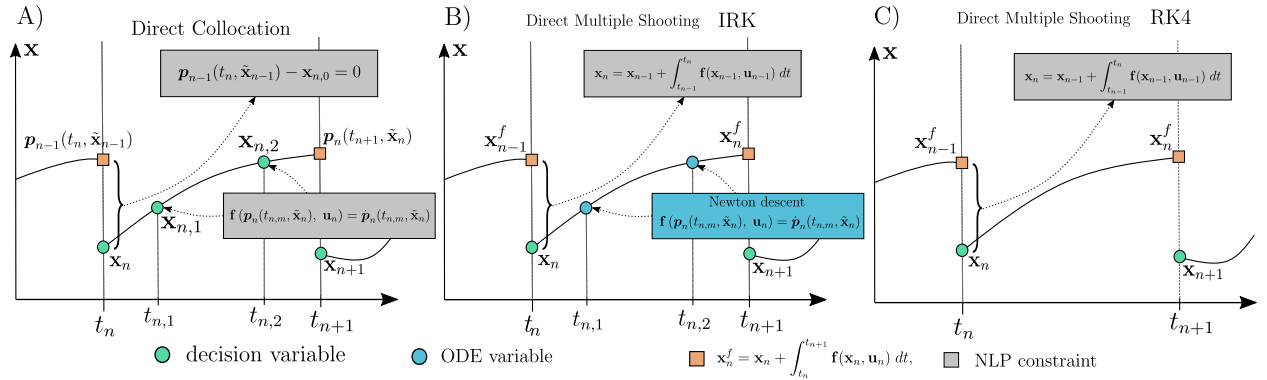


Figure 1: Illustrations of OCP transcriptions. A) Direct Collocation, B) Direct multiple shooting with IRK, C) Direct multiple Shooting.

### 2.4 Rigid-body dynamics constraints

In the previous sections, we have introduced two transcriptions methods for trajectory optimization, namely, DC and DMS. As presented, they can be declined into several formulations (changing polynomials for DC, changing integrators for DMS), and some parallels can be drawn between them. In the following, we propose to investigate the behavior of a subset of selected formulations, namely: (i) DMS with explicit ERK, (ii) DMS with IRK, and (iii) DC with Lagrange polynomials. The same Legendre polynomials of order 4 will be considered for DMS with IRK, and DC.

In the case of rigid-body dynamics, the dynamics constraint Eq. (1c) of a multibody system, with generalized coordinates  $\mathbf{q}$ , velocities  $\dot{\mathbf{q}}$ , and accelerations  $\ddot{\mathbf{q}}$  is:

$$M(\mathbf{q})\ddot{\mathbf{q}} + N(\mathbf{q}, \dot{\mathbf{q}}) = S^\top \boldsymbol{\tau}_J, \quad (6)$$

where  $M(\mathbf{q})$  is the mass matrix,  $N(\mathbf{q}, \dot{\mathbf{q}})$  is the vector of nonlinear effects and gravity,  $\boldsymbol{\tau}_J$  is the joint torques vector, and  $S$  the selection matrix. By letting the state and control vectors be  $\mathbf{x} = [\mathbf{q}, \dot{\mathbf{q}}]$  and  $\mathbf{u} = \boldsymbol{\tau}_J$  respectively, this equation can be rewritten as an ODE of the form  $\dot{\mathbf{x}} = \mathbf{f}(\mathbf{x}, \mathbf{u})$  to match the previously introduced equations.

Concerning DMS with IRK and DC, two ways to compute the dynamics constraints will be presented (Eqs. 8 and 9). At each knot interval  $[t_n, t_{n+1}]$ , the states trajectory  $\mathbf{x}$  is modeled by a polynomial  $\mathbf{p}_n$ , concatenating the generalized coordinates polynomial  $\mathbf{p}_n^q$  and the generalized velocities polynomial  $\mathbf{p}_n^{\dot{q}}$ . The generalized accelerations polynomial is directly derived from  $\mathbf{p}_n^{\dot{q}}$  as  $\mathbf{p}_n^{\ddot{q}}(t) = \dot{\mathbf{p}}_n^{\dot{q}}(t)$ ,  $\forall t$ . At *collocation points*, the first constraint ensures that the derivative of the generalized coordinates polynomial matches the generalized velocities polynomial:

$$\forall t_{n,m}, \mathbf{p}_n^{\dot{q}}(t_{n,m}, \tilde{\mathbf{x}}_n) = \dot{\mathbf{p}}_n^q(t_{n,m}, \tilde{\mathbf{x}}_n). \quad (7)$$

The consistency of the generalized coordinates, velocity, and acceleration polynomials can be constrained through forward dynamics (FD), as written in Eq. 3, or through inverse dynamics (ID), by rearranging the terms the equations:

$$\forall t_{n,m}, FD(\mathbf{p}_n^q(t_{n,m}, \tilde{\mathbf{x}}_n), \mathbf{p}_n^{\dot{q}}(t_{n,m}, \tilde{\mathbf{x}}_n), \boldsymbol{\tau}_n) - \mathbf{p}_n^{\ddot{q}}(t_{n,m}, \tilde{\mathbf{x}}_n) = \mathbf{0}, \quad (8)$$

$$\forall t_{n,m}, ID(\mathbf{p}_n^q(t_{n,m}, \tilde{\mathbf{x}}_n), \mathbf{p}_n^{\dot{q}}(t_{n,m}, \tilde{\mathbf{x}}_n), \mathbf{p}_n^{\ddot{q}}(t_{n,m}, \tilde{\mathbf{x}}_n)) - \boldsymbol{\tau}_n = \mathbf{0}. \quad (9)$$

Eq. 8 amounts to matching joint accelerations with forward dynamics ( $\ddot{\mathbf{q}} - FD(\mathbf{q}, \dot{\mathbf{q}}, \boldsymbol{\tau}) = 0$ ), with  $FD$  the forward dynamics algorithm using the articulated body algorithm (ABA), *i.e.*, without numerical inversion of the mass matrix [Featherstone, 1999]. Eq. 9 amounts to matching torques with inverse dynamics ( $\boldsymbol{\tau} - ID(\mathbf{q}, \dot{\mathbf{q}}, \ddot{\mathbf{q}}) = 0$ ), with  $ID$  the inverse dynamics using the recursive Newton-Euler algorithm (RNEA, [Featherstone, 1987]). Both algorithms run in time  $O(n)$ , RNEA (ID) algorithm is expected to be faster since it relies on a two-pass algorithm, whereas ABA (FD) has three recursive loops. The two formulations will be investigated in the following.

### 3 Methods

Five OCPs, involving models of increasing complexity (from 3 to 15 DoFs; Fig. 2 and Table 1), were used to compare the performances of the transcription methods. The number of knot points (Table 1) was adjusted to ensure good convergence properties for each OCP, according to our experience [Bailly et al., 2021a, Puchaud et al., 2023] at least 100 knot points per second.

As frequently done in biomechanics, the rigid-body models were either actuated by muscles or by joint torques. The initial and final states of the OCPs were bounded and/or constrained. All the tasks are briefly described below and detailed in A.

Table 1: Summary of the five OCPs

OCP	1	2	3	4	5
<b>Model</b>	Leg	Arm	Upper limb	Planar human	Acrobat
<b># DoFs</b>	3	6	10	12	15
<b>Dynamics</b>	Torque-driven	Torque-driven	Muscle-driven with residual torques	Torque-driven with contact	Torque-driven
<b># Actuators</b>	3	6	26 + 10	9	9
<b>Forward Dynamics (ABA)<sup>a</sup> (<math>\mu</math>s)</b>	8.1	9.7	13	12	15
<b>Inverse Dynamics (RNEA)<sup>a</sup> (<math>\mu</math>s)</b>	6.4	7.5	9.8	9.3	11
<b>Knot points</b>	20	50	100	30	125
<b>Final time (s)</b>	0.25	0.25	1.0	0.3	1.5 $\pm$ 0.05

Notes: <sup>a</sup> Reported dynamics computation time is averaged over  $10^5$  function calls.

#### 3.1 Rigid-body models and task

The following models were inferred from real systems or adapted from the literature:

*OCPI* A 3-DoF hexapod leg Robotis BIOLOID was modeled as in Trivun et al. [2017], using three hinge joints (Z-Y-Y). The task was to move the end-effector between two set positions while minimizing joint torques (primarily) and joint velocities (secondary).

- OCP2* A 4-body, 6-DoF arm model was adapted from Docquier et al. [2019]. The first body is connected to the base with two hinges. The second and third bodies are connected through a single hinge joint. The last body is an inverted pendulum connected through a universal joint on the third body. A reaching task was simulated, maintaining the pendulum vertical at the beginning, and the end of the task similarly to Docquier et al. [2019], by mainly minimizing joint torques and their time derivatives.
- OCP3* A 5-body, 10-DoF upper-limb musculoskeletal model was derived from Wu et al. [2016]. The sternoclavicular joint was modeled as a universal joint. The acromioclavicular and glenohumeral joints were modeled as 3-DoF ball-and-socket joints. The forearm and wrist were modeled as body segments connected to the elbow via a universal joint. Twenty-six muscle units represented the major muscle groups of the shoulder complex. A reaching task was simulated to move the hand between two set positions, while minimizing joint torques, joint velocities, and their respective rates of change.
- OCP4* A 12-DoFs planar human model (83 kg, 1.67 m) was implemented in line with Serrancolí and Pàmies-Vilà [2019]. The torso segment was the free-floating base with three DoFs. The neck, the left, and right hips, knees, shoulders, and elbows were revolute actuated joints. Half a gait cycle was simulated. Joint torques and joint accelerations were minimized.
- OCP5* A 15-DoFs full human body was modeled (male, 18 years old, 73.6 kg, 170.8 cm) [Puchaud et al., 2023]: 6 unactuated DoFs for the floating base, 3 for the thoracolumbar joint (flexion, lateral flexion, and axial rotation), 2 for each shoulder (plane of elevation and elevation), and 2 for the right and left hips (flexion and abduction). The inertial parameters were based on 95 anthropometric measures on an elite trampolinist, in line with Yeadon’s anthropometric model [Yeadon, 1990]. A  $1\frac{3}{4}$  somersault with one twist was simulated from a trampoline bed until a pre-landing position, similarly to Puchaud et al. [2023]. A multi-objective function included the joint torques and the rate of change of joint velocities.

### 3.2 Transcriptions of the optimal control problems

Five OCP transcriptions were compared, three of them belonging to direct multiple shooting schemes:

- explicit 4th-order Runge-Kutta with five intermediate steps (*MSE*),
- implicit Runge-Kutta with rigid-body dynamics constraints based on forward dynamics (*MSI<sup>FD</sup>*),
- implicit Runge-Kutta with rigid-body dynamics constraints based on inverse dynamics (*MSI<sup>ID</sup>*),

and the remaining two, belonging to direct collocation schemes:

- rigid-body dynamics constraints based on forward dynamics (*DC<sup>FD</sup>*),
- rigid-body dynamics constraints based on inverse dynamics (*DC<sup>ID</sup>*).

A fourth-order polynomial of Legendre was used as a time grid for IRK and collocation.

The planar human *OCP4* was not run with implicit dynamics as it required a specific formulation of inverse dynamics to include non-acceleration constraints at contact points (a feature not available in the Biotrim library yet).

Table 2: Size of the NLPs resulting from the transcription methods (DMS vs DC), for the five OCPs

OCP Model	1 Leg		2 Arm		3 Upper limb		4 Planar human		5 Acrobat	
	DMS	DC	DMS	DC	DMS	DC	DMS	DC	DMS	DC
states	126	606	612	3012	2020	2020	744	3624	3780	18780
controls	60	60	300	300	3600	3600	360	360	1125	1125
parameters	0	0	0	0	0	0	0	0	1	1
equality constraints	132	612	621	3021	2000	10020	732	3612	4880	18750
<i>nzt</i> in equality jacobian	1111	4734	10805	52316	107800	343950	24395	66250	142182	382370
inequality constraints	0	0	0	0	0	0	32	32	0	0
<i>nzt</i> in inequality jacobian	0	0	0	0	0	0	1008	1008	0	0
Lagrangian Hessian	762	1703	7833	38004	144318	364098	48915	94035	118149	291048

Notes: *nzt* stands for non-zero terms. Lagrangian Hessian refers to the cost function.

### 3.3 Multi-start approach

All OCPs were implemented in Biotrim [Michaud et al., 2022], an optimal control toolbox for biomechanics that implements both DMS and DC transcriptions. The code is available online [Puchaud, 2023]. The OCPs were run on an AMD Ryzen 9 5950X processor with 128 Go RAM; OCPs were parallelized on eight threads, four OCPs running in parallel. The problem was solved using IPOPT with exact Hessian [Wächter and Biegler, 2006], ma57 linear solver [Duff, 2004], and CasAdi for algorithmic differentiation [Andersson et al., 2019]. Convergence and constraint tolerances were set to  $10^{-6}$  and  $10^{-4}$ , respectively. Since solving such NLPs may result in finding local minima, each NLP was solved 100 times using random noise applied to the initial guesses, whose magnitudes were specific for each OCP (Table 1). All solutions were considered for further analysis.

### 3.4 Analysis

For each OCP, we compared the convergence rates, the convergence times, and the values of the cost function at convergence resulting from each transcription. We reported their medians as they give a better sense of non-uniformly distributed data. Dynamic consistency was evaluated through the root mean square error between optimal and re-integrated generalized coordinates at final time  $t_f$ . Re-integrated solutions were obtained by solving an initial value problem, starting from the state at  $t_0$ , and integrating forward in time the optimized control trajectory using optimized control with the variable-step explicit Runge-Kutta method of order 8(5,3) (Hairer and Wanner 1996, DOP853), implemented in *scipy*. Relative and absolute tolerances were set to  $1e^{-3}$  and  $1e^{-6}$ , respectively. This choice of tolerances was made to ensure a high level of accuracy in the re-integration.

## 4 Results

**Convergence rate.** Convergence rates for OCP1 to OCP5 were 98.2%, 99.4%, 100%, 100% and 100% . For OCP1, only nine simulations failed to converge ( $MSE$ : 1,  $MSI^{FD}$ : 2,  $MSI^{ID}$ : 2,  $DC^{FD}$ : 2,  $DC^{ID}$ : 2) and only three simulations for OCP2 ( $MSE$ : 1,  $MSI^{FD}$ : 1,  $MSI^{ID}$ : 1). The trials that failed to converge were excluded from the subsequent analyses.

**CPU Time.** Overall, none of the five transcriptions was faster for all OCPs. On the one hand, DMS transcriptions were faster than DC for OCP2 and OCP5,  $MSI^{ID}$  being the fastest for OCP2. On the other hand, DC was faster than DMS for OCP1, OCP4, and OCP3. Among each problem, for the inverse dynamics rigid-body constraints, the median CPU times of  $MSI^{ID}$  and  $DC^{ID}$  were similar to or lower than their corresponding forward dynamics versions ( $MSI^{FD}$  and  $DC^{FD}$ ). For OCP1 and OCP2,  $MSI^{ID}$  was faster than  $MSI^{FD}$  by 1.15 and 1.82 times, respectively. For OCP3, the two methods performed similarly. Also,  $DC^{ID}$  was faster than  $DC^{FD}$  for OCP1, OCP3, and OCP5 by 1.03, 1.12, and 1.56 times respectively, except for OCP2, where  $DC^{FD}$  was 1.14 times faster.

**Optimality.** All transcriptions led to similar optima. For OCP1, two solutions in  $DC^{FD}$  converged to a higher local minimum ( $7.4 \text{ e-}4$  instead of  $7.2 \text{ e-}4$ ), and for OCP4, four solutions (2 in  $MSE$ , 2 in  $MSI^{FD}$ ) converged to a higher local minimum (3691 instead of 884). The OCP2 presented two clusters of optimal solutions. For each transcription, the first cluster contained 63% to 68% of the optimal solutions ( $DC^{ID}$  and  $DC^{FD}$ , respectively). In other words, all transcription methods performed similarly. For OCP5, the cost values were more scattered.  $MSE$ ,  $MSI^{ID}$ , and  $MSI^{FD}$  led to similar local minima, but  $DC^{FD}$  showed a larger variability with a lower median. Furthermore,  $DC^{ID}$  led to a lower variability. Finally, the lowest minima were found by DMS transcriptions, but these solutions presented one of the lowest dynamic consistency compared to other local minima, see Fig. 4.

**Dynamic Consistency.** In general,  $MSI^{FD}$ ,  $MSI^{ID}$ ,  $DC^{FD}$ , and  $DC^{ID}$  led to lower errors than  $MSE$  after re-integrating the optimal solution using DOP853. Errors were the highest for  $MSE$  in OCP2, 4, and 5. Moreover,  $MSE$  led to RMSE errors up to  $100^\circ$  by the end of the simulation of OCP5, even though these solutions were related to the lowest local minima found with all transcriptions. Thus,  $MSI^{FD}$ ,  $MSI^{ID}$ ,  $DC^{FD}$ , and  $DC^{ID}$  solutions are more dynamically consistent than  $MSE$ .

## 5 Discussion

This study aimed to evaluate the performance of various direct optimal control transcriptions and dynamic formulations on five OCPs, related to rigid-body dynamics and biomechanics. We found that the five OCPs of increasing complexity (including torque-driven, and muscle-driven dynamics) were solved in a similar amount of CPU time, whatever the transcription. Among the transcriptions, those incorporating implicit dynamics, such as DMS with IRKs or DC, preserved dynamic consistency better. Rigid-body dynamics constraints based on inverse dynamics slightly hastened the convergence.

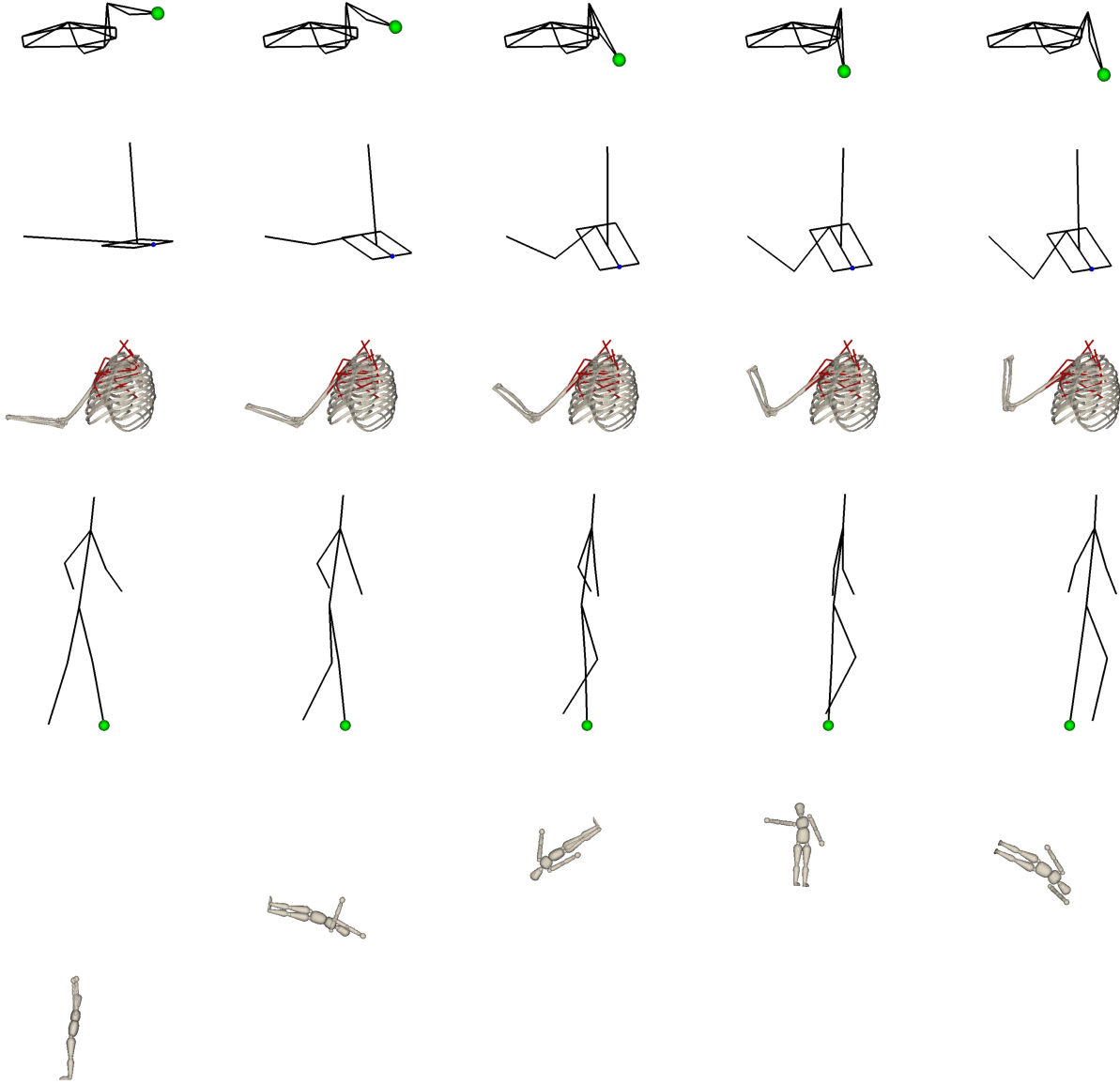


Figure 2: Illustrations of results of five OCPs, from 1 to 5 (top to bottom).

### 5.1 Limitations and strengths

We will discuss these findings in line with two main limitations. First, a good initial guess helps the NLP solver to converge toward an optimal solution. However, all examples were treated as predictive simulations without *a priori* knowledge of the solution. Interior-point algorithms are more robust than SQP solvers to such poor initial guesses [Betts, 2010]. Nevertheless, SQP solvers are well designed to solve DMS and DC quickly, Acados [Verschuere et al., 2022] being a good example for real-time applications. In the present study, we only used one interior-point solver, IPOPT, commonly used in biomechanics [Dembia et al., 2020, Lee and Umberger, 2016, Bailly et al., 2021b]. Since performances depend on the NLP solver, our findings cannot be extrapolated to other interior-point or SQP algorithms.

Secondly, our DMS implementation did not correspond to the state-of-the-art algorithm of Bock and Plitt [1984]. The DMS transcription in Biopotim is mainly based on various fixed-step ERK and IRK. In contrast, a strong feature of DMS is to rely on an adaptive step size ODE solver to control the accuracy of the dynamics without changing the size

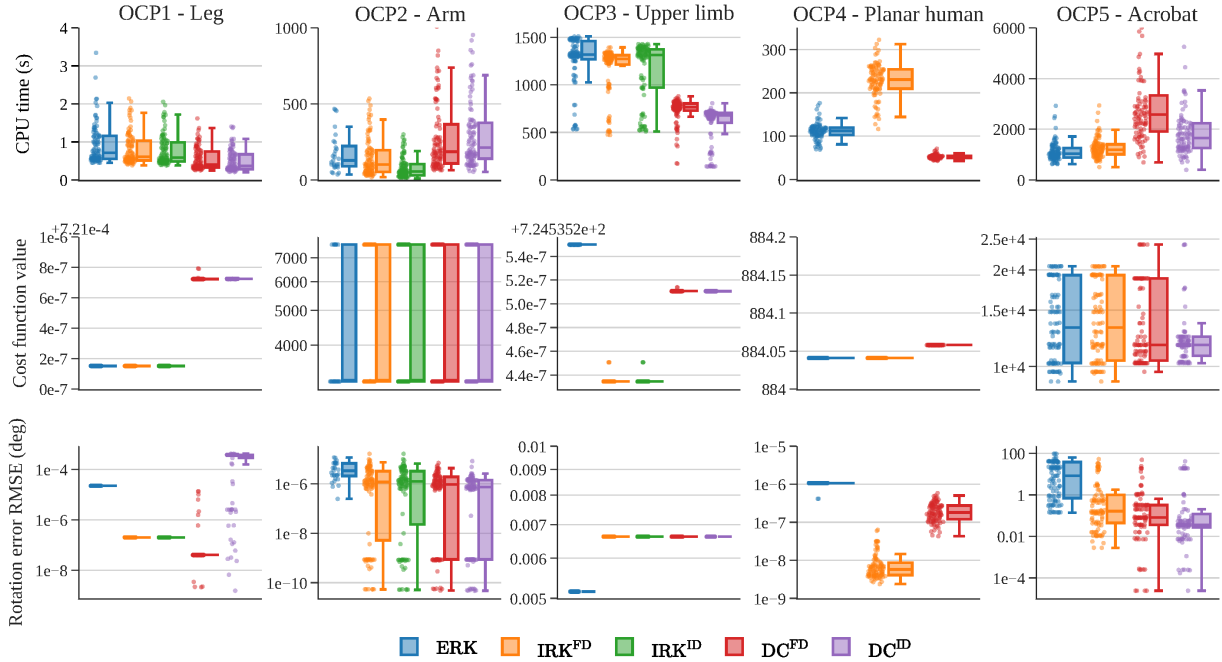


Figure 3: CPU time, cost function values, and dynamic consistency for each OCP and each transcription. The y-axes have a logarithmic scale for cost function values and dynamic consistency. A Html version of the figure is available as supplementary material to further explore the data.

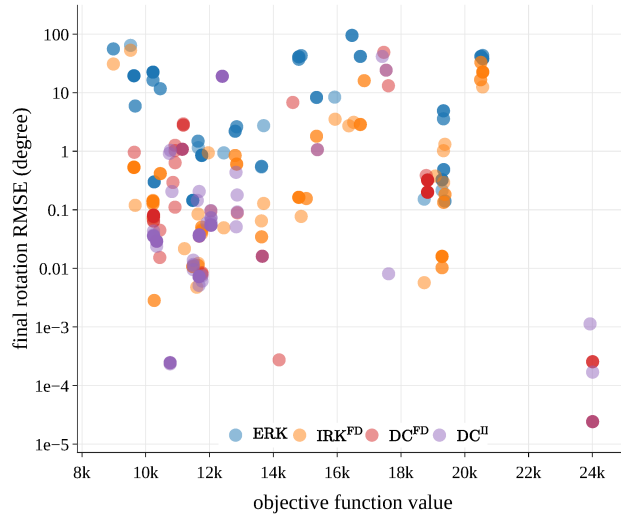


Figure 4: Cost versus dynamic consistency for OCP5. The dynamics consistency y-axis has a logarithmic scale. A Html version of the figure is available as supplementary material to further explore the data.

of the NLP problem. On the contrary, DC requires mesh refinements to improve the dynamic consistency, changing the problem size. Fixed-step ODE solvers are more convenient and efficient for algorithmic differentiation. While Bioptim (through CasADI, Andersson et al. 2019) is connected to CVODES [Serban and Hindmash, 2008], a solver with sensitivity analysis capabilities, our experience with this solver resulted in a significant increase in CPU times.

Nevertheless, the 4th order polynomial and fixed-step size result in errors less than  $0.01^\circ$  in 4 out of 5 OCPs, by the end of the simulation compared to the explicit Runge-Kutta method of order 8(5,3) DOP853. We believe these dynamical errors below  $1^\circ$  are accurate enough for predictive simulation in biomechanics. As shown in Sec. 2, having fixed-step ODE solvers (5-step RK4 and 4th order Legendre collocation) reduces the difference between DMS and DC implementations on two aspects: (i) where the dynamics constraints are solved (ODE solver *versus* NLP solver, respectively); (ii) the number of NLP variables and constraints (collocation points being bounded in DC). Consequently, this led to similar results in the present study.

Despite these two limitations, the strengths of the present study should be acknowledged. First, we included various OCPs with increasing complexity from 3 to 15 DoFs, requiring from 0.45 to 1366 seconds to be solved. We included torque-driven and muscle-driven dynamics, and NLPs had a significant problem size with equality constraints ranging from 132 to 10 020. Within this diversity, no clear conclusion can be drawn, showing that the best transcription cannot be anticipated in the context of trajectory optimization for multibody systems. According to Febrer-Nafría et al. [2022] review, most studies considered the performance of their optimal control transcription based on a single transcription and one model. Even if we did not reach the complexity of some OCP available in the literature, up to 31 DoFs and 92 muscles [Falisse et al., 2022], our study provides a more comprehensive perspective.

Second, the transcriptions were all coded using the same software, Biotim. All transcription methods differ by only two instructions (see code repository [Puchaud, 2023]). Having a unique modeler and unique software to compare transcriptions greatly reduces the bias and possibility of errors from hand-coded scripts, lacking support for versatility formulations [Lee and Umberger, 2016, Koelewijn and van den Bogert, 2020, Febrer-Nafría et al., 2021]. Additionally, the Lagrangian cost functions in both DMS and DC were computed with the same Euler forward approximation, making the software differences between DMS with IRK and DC minimal. Any variations in performance can thus be attributed to the fundamental differences between the two transcription approaches. This lack of homogeneity in implementations led to large differences in performance in inverse approach with musculoskeletal models [Kim et al., 2018]. Other software used for optimal control in biomechanics, such as Moco [Dembia et al., 2020] or Muscod II [Leineweber et al., 2003] only provide a DC or a DMS solver. Only a few software enable solving OCPs with DMS and DC, such as Horizon [Ruscelli et al., 2022], CasAdos [Frey et al., 2022], and Biotim being specifically tailored multibody systems including biomechanics [Michaud et al., 2022].

## 5.2 CPU time to convergence

In the literature, predictive simulations with musculoskeletal models converge between 10 min to 100 h [Febrer-Nafría et al., 2022]. In our case, the upper limb musculoskeletal model took up to 25 min to converge. Full-body acrobat model with 15 DoFs (OCP4) had medians from 17.3 to 42.9 min CPU time and maximally reached 1.6 hours to converge. These CPU time were quite low, probably because no contact mechanics was considered. In our case, CPU times to solve OCPs were similar for DMS and DC. In contrast, Porsa et al. [2016] reported that direct single shooting was 249 times slower than DC. It may not be appropriate to compare direct single shooting with DC or DMS in terms of computational efficiency, so this transcription was not considered in the present paper. Indeed, The DMS transcription has been initially developed to leverage the issue that rises from the direct single shooting transcription [Bock and Plitt, 1984]. In our case, CPU times were similar for DMS and DC, DC was about 5 times lower than DMS in OCP4 and 4 times higher in OCP2. None of the transcriptions consistently showed a faster convergence among these five examples, and no other clear cause was found, other than the transcriptions being similar as presented in Sec. 2.

Nonetheless, inverse dynamics constraints usually led to faster convergence. In all cases but OCP3, transcriptions based on inverse dynamics constraints ( $MSI^{ID}$  and  $DC^{ID}$ ) resulted in faster convergence than forward dynamics constraints ( $MSI^{FD}$  and  $DC^{FD}$ ). It confirms the hypothesis made in Sec. 2.4 and strengthens previous findings [Puchaud et al., 2023, Ferrolho et al., 2021]. Running the forward dynamics function took around 1.3 times longer than the inverse dynamics function for our multibody models (Table 1). This ratio was never reached when comparing the time to converge between transcriptions ( $MSI^{FD}$  vs  $MSI^{ID}$ , and  $DC^{FD}$  vs  $DC^{ID}$ ). Indeed, most of the time is spent evaluating the Lagrangian Hessian and the constraint Jacobian, not necessarily calling the dynamics function. Still, we recommend the use of inverse dynamics defects when possible.

Finally, the initial guess has a significant impact on CPU time. An initial guess that converges quickly with one transcription does not guarantee that another initial guess will converge as fast. Moreover, an initial guess that converges quickly, does not guarantee similar results with another transcription. Therefore, the variation in CPU time can be attributed more to the initial solution rather than the transcription method used. If possible, we suggest providing a minimally data-informed solution to reduce the CPU time to convergence for predictive simulation in biomechanics, such as for OCP3, 4, and 5 in the present study. But most importantly, to fairly compare different transcriptions, we suggest employing a multi-start approach.

### 5.3 Optimality

Three interesting behaviors emerged from the present study’s five OCP examples. In OCP1, 3, and 4, a unique optimal solution was found, whatever the transcription method and the initial guess. The cost values (Fig. 3), states, and controls, were nearly identical. The cost function was simple enough almost to admit a unique solution. The anecdotal differences in the cost between the methods may be explained by the slight change in dynamic consistency (cost increasing when consistency decreasing) or by the Karush–Kuhn–Tucker (KKT) conditions being different by construction between DMS and DC while the exit tolerance ( $1e-6$ ) was the same.

In OCP2, two clusters of solutions were found, one being a sub-optimum. Again, since the proportion of global *versus* local optima were similar between the methods (from 63% to 68%), our recommendation is to use a multi-start approach whatever the transcription methods or to have an *a priori* knowledge of the solution.

In OCP5, several local minima were found for all the transcription methods. Finding a variety of local minima is usual in optimal control and specifically in biomechanics [Falisse et al., 2019, Gidley et al., 2018]. Indeed, the objective function may include several terms, such as metabolic cost, muscle torque, stability, and penalty regularization. The weighting of these multi-objective functions is challenging, as they are usually manually fine-tuned [Brown and McPhee, 2020, Febrer-Nafria et al., 2021, Felis and Mombaur, 2016]. Thus, these complex objective functions may compensate each other, and, with different initial guesses, they may converge toward different optima. Nonetheless, whatever the transcription, local minima can be found, and local minima can be similar.

The present study does not support the finding: Docquier et al. [2019] found that rigid-body dynamics constraints based on forward dynamics lead to worse local optimal solutions than the constraints based on inverse dynamics. In OCP5,  $DC^{ID}$  led to lower local minima, and OCPs converged to the same optima. Further studies are needed to explore the effect of rigid-body dynamics constraints on optimality. However, it is worth noting that the most optimal solutions showed low dynamic consistency. Indeed, the best solutions in terms of cost (see Fig. 4) presented low dynamic consistency (re-integration error higher than  $1^\circ$  and up to  $100^\circ$  in  $MSE$ ). Thus, evaluating only the quantity of low local minima can be misleading as the optimal solution can be dynamically inconsistent since the transcriptions may exploit its weaknesses to get better cost function value.

### 5.4 Dynamic consistency

Dynamic consistency is the criterion that showed the largest differences between the transcriptions, especially  $MSE$  *versus* the collocation-based methods (IRK and DC). IRK based on 4th-order Legendre polynomials provided consistent dynamics for all simulations. Both  $MSI^{ID}$  and  $MSI^{FD}$  based on Legendre collocation time-grid showed reliable dynamic consistency for the presented OCPs, and,  $MSE$  showed the largest errors, especially for OCP5.

IRKs are efficient when solving OCPs with SQP methods [Quirynen et al., 2015]. For predictive simulations, implicit integrators are recommended since they better control the integration error and, consequently, the dynamic consistency. Further analyses should be made to compare the result with adaptive step size ODE solvers to characterize DMS transcription better to exclude the use of direct multiple shooting with explicit ODE solvers for predictive simulation. These results strengthen previous recommendations to use implicit dynamics [Van Den Bogert et al., 2011, De Groot et al., 2016], but do not exclude DMS as a transcription. Another type of integrators may also be considered to enhance dynamic consistency, namely symplectic ODE solvers such as Leapfrog integrator [Ruscelli et al., 2022], or variational integrators that rely on discrete mechanics [Johnson and Murphey, 2009] and may be beneficial for their energy conservation properties for biomechanical motions which last longer than 1 s (e.g., diving or repetitive tasks).

## 6 Conclusion

Our study highlights that the five transcriptions, including DMS and DC, took similar CPU time to solve the five OCPs related to rigid-body dynamics. To effectively compare the different transcriptions, we suggest utilizing a multi-start approach and a variety of examples. Among the transcriptions we evaluated, those incorporating implicit dynamics, such as direct multiple shooting with IRKs or direct collocation, were particularly effective in finding optimal solutions and preserving dynamic consistency. Additionally, we recommend employing rigid-body dynamics constraints based on inverse dynamics when available to gain extra time for convergence. We recommend using frameworks to facilitate this process and identify the most suitable transcription method for a given OCP.

## 7 Acknowledgment

The NSERC Discovery grant of Mickaël Begon (RGPIN-2019-04978) funded this study.

## References

- Moritz Diehl, Hans Georg Bock, Holger Diedam, and P. B. Wieber. Fast direct multiple shooting algorithms for optimal robot control. In *Lecture Notes in Control and Information Sciences*, volume 340, pages 65–93, 2006. ISBN 3540361189. doi:10.1007/978-3-540-36119-0\_4.
- Míriam Febrer-Nafría, Ali Nasr, Mahdokht Ezati, Peter Brown, Josep M. Font-Llagunes, and John McPhee. Predictive multibody dynamic simulation of human neuromusculoskeletal systems: a review. *Multibody System Dynamics 2022*, pages 1–41, 11 2022. ISSN 1573-272X. doi:10.1007/S11044-022-09852-X.
- Matthew Kelly. An introduction to trajectory optimization: How to do your own direct collocation. *SIAM Review*, 59(4):849–904, 2017. ISSN 00361445. doi:10.1137/16M1062569.
- John T. Betts. *Practical Methods for Optimal Control and Estimation Using Nonlinear Programming*. Society for Industrial and Applied Mathematics, 1 2010. doi:10.1137/1.9780898718577.
- Markus Gifftthaler, Michael Neunert, Markus Stauble, Jonas Buchli, and Moritz Diehl. A Family of Iterative Gauss-Newton Shooting Methods for Nonlinear Optimal Control. *IEEE International Conference on Intelligent Robots and Systems*, pages 6903–6910, 12 2018. ISSN 21530866. doi:10.1109/IROS.2018.8593840.
- Jean Pierre Sleiman, Jan Carius, Ruben Grandia, Martin Wermelinger, and Marco Hutter. Contact-Implicit Trajectory Optimization for Dynamic Object Manipulation. *IEEE International Conference on Intelligent Robots and Systems*, pages 6814–6821, 11 2019. ISSN 21530866. doi:10.1109/IROS40897.2019.8968194.
- Mahdokht Ezati, Borna Ghannadi, and John McPhee. A review of simulation methods for human movement dynamics with emphasis on gait. *Multibody System Dynamics*, 47(3):265–292, 2019. ISSN 1573272X. doi:10.1007/s11044-019-09685-1.
- Míriam Febrer-Nafría, Roger Pallarès-López, Benjamin J. Fregly, and Josep M. Font-Llagunes. Comparison of different optimal control formulations for generating dynamically consistent crutch walking simulations using a torque-driven model. *Mechanism and Machine Theory*, 154, 2020. ISSN 0094114X. doi:10.1016/j.mechmachtheory.2020.104031.
- Leng Feng Lee and Brian R. Umberger. Generating optimal control simulations of musculoskeletal movement using OpenSim and MATLAB. *PeerJ*, 2016(1):e1638, 1 2016. ISSN 21678359. doi:10.7717/PEERJ.1638/FIG-6.
- Thomas Geijtenbeek. SCONE: Open Source Software for Predictive Simulation of Biological Motion. *Journal of Open Source Software*, 4(38):1421, 6 2019. ISSN 2475-9066. doi:10.21105/joss.01421.
- H. G. Bock and K. J. Plitt. A Multiple Shooting Algorithm for Direct Solution of Optimal Control Problems. *IFAC Proceedings Volumes*, 17(2):1603–1608, 7 1984. doi:10.1016/S1474-6670(17)61205-9.
- André Venne, François Bailly, Eve Charbonneau, Jennifer Dowling-Medley, and Mickaël Begon. Optimal estimation of complex aerial movements using dynamic optimisation. *Sport Biomechanics*, pages 1–16, 6 2022. doi:10.1080/14763141.2022.2066015.
- Jens Koschorreck and Katja Mombaur. Modeling and optimal control of human platform diving with somersaults and twists. *Optimization and Engineering*, 13(1):29–56, 10 2012. doi:10.1007/s11081-011-9169-8.
- Eve Charbonneau, François Bailly, Loane Danès, and Mickaël Begon. Optimal control as a tool for innovation in aerial twisting on a trampoline. *Applied Sciences (Switzerland)*, 10(23):1–17, 11 2020. doi:10.3390/app10238363.
- Martin L. Felis and Katja Mombaur. Synthesis of full-body 3-D human gait using optimal control methods. In *Proceedings - IEEE International Conference on Robotics and Automation*, volume 2016-June, pages 1560–1566. Institute of Electrical and Electronics Engineers Inc., 6 2016. doi:10.1109/ICRA.2016.7487294.
- Manish Sreenivasa, Matthew Millard, Martin Felis, Katja Mombaur, and Sebastian I. Wolf. Optimal control based stiffness identification of an ankle-foot orthosis using a predictive walking model. *Frontiers in Computational Neuroscience*, 11(April), 2017. doi:10.3389/fncom.2017.00023.
- Monika Harant, Manish Sreenivasa, Matthew Millard, Nejc Sarabon, and Katja Mombaur. Parameter optimization for passive spinal exoskeletons based on experimental data and optimal control. *IEEE-RAS International Conference on Humanoid Robots*, pages 535–540, 12 2017. doi:10.1109/HUMANOIDS.2017.8246924.
- Manish Sreenivasa, Matthew Millard, Idsart Kingma, Jaap H. van Dieën, and Katja Mombaur. Predicting the influence of hip and lumbar flexibility on lifting motions using optimal control. *Journal of Biomechanics*, 78:118–125, 9 2018. doi:10.1016/J.JBIOMECH.2018.07.028.
- Lorenz T. Biegler. Solution of dynamic optimization problems by successive quadratic programming and orthogonal collocation. *Computers & Chemical Engineering*, 8(3-4):243–247, 1 1984. doi:10.1016/0098-1354(84)87012-X.
- Yi Chung Lin and Marcus G. Pandy. Three-dimensional data-tracking dynamic optimization simulations of human locomotion generated by direct collocation. *Journal of Biomechanics*, 59:1–8, 7 2017. doi:10.1016/J.JBIOMECH.2017.04.038.

- Marko Ackermann and Antonie J. van den Bogert. Optimality principles for model-based prediction of human gait. *Journal of Biomechanics*, 43(6):1055–1060, 4 2010. doi:10.1016/J.JBIOMECH.2009.12.012.
- Ross H. Miller and Joseph Hamill. Optimal footfall patterns for cost minimization in running. *Journal of Biomechanics*, 48(11):2858–2864, 8 2015. doi:10.1016/J.JBIOMECH.2015.04.019.
- Antoine Falisse, Maarten Afschrift, and Friedl De Groote. Modeling toes contributes to realistic stance knee mechanics in three-dimensional predictive simulations of walking. *Plos One*, 17(1):e0256311, 2022. doi:10.1371/journal.pone.0256311.
- Henrique Ferrolho, Vladimir Ivan, Wolfgang Merkt, Ioannis Havoutis, and Sethu Vijayakumar. Inverse Dynamics vs. Forward Dynamics in Direct Transcription Formulations for Trajectory Optimization. *Proceedings - IEEE International Conference on Robotics and Automation*, 2021-May:12752–12758, 2021. doi:10.1109/ICRA48506.2021.9561306.
- Antonie J. Van Den Bogert, Dimitra Blana, and Dieter Heinrich. Implicit methods for efficient musculoskeletal simulation and optimal control. *Procedia IUTAM*, 2:297–316, 2011. doi:10.1016/j.piutam.2011.04.027.
- Friedl De Groote, Allison L. Kinney, Anil V. Rao, and Benjamin J. Fregly. Evaluation of Direct Collocation Optimal Control Problem Formulations for Solving the Muscle Redundancy Problem. *Annals of Biomedical Engineering*, 44(10):2922–2936, 2016. doi:10.1007/s10439-016-1591-9.
- Pierre Puchaud, Eve Charbonneau, Benjamin Michaud, and Mickaël Begon. Optimality equivalence and computational advantages of free-floating base dynamics compared to full-body dynamics. *Mechanism and Machine Theory*, 181:105164, 3 2023. doi:10.1016/J.MECHMACHTHEORY.2022.105164.
- Quentin Docquier, Olivier Brüls, and Paul Fiset. Comparison and analysis of multibody dynamics formalisms for solving optimal control problem. In *IUTAM Bookseries*, volume 33, pages 55–77. Springer, Cham, 2019. doi:10.1007/978-3-030-00527-6\_3.
- Antoine Falisse, Gil Serrancolí, Christopher L. Dembia, Joris Gillis, Ilse Jonkers, and Friedl De Groote. Rapid predictive simulations with complex musculoskeletal models suggest that diverse healthy and pathological human gaits can emerge from similar control strategies. *Journal of the Royal Society Interface*, 16(157), 8 2019. doi:10.1098/RSIF.2019.0402.
- Eve Charbonneau, François Bailly, and Mickaël Begon. Optimal forward twisting pike somersault without self-collision. *Sports Biomechanics*, 22(special issue Biomechanics of Acrobatic Sports):1–18, 3 2022. doi:10.1080/14763141.2022.2052348.
- Joel A.E. Andersson, Joris Gillis, Greg Horn, James B. Rawlings, and Moritz Diehl. CasADi: a software framework for nonlinear optimization and optimal control. *Mathematical Programming Computation*, 11(1):1–36, 3 2019. doi:10.1007/S12532-018-0139-4/TABLES/3.
- Radu Serban and Alan C. Hindmarsh. CVODES: The Sensitivity-Enabled ODE Solver in SUNDIALS. *Proceedings of the ASME International Design Engineering Technical Conferences and Computers and Information in Engineering Conference - DETC2005*, 6 A:257–269, 6 2008. doi:10.1115/DETC2005-85597.
- Michael A. Patterson and Anil V. Rao. GPOPS-II. *ACM Transactions on Mathematical Software (TOMS)*, 41(1), 10 2014. doi:10.1145/2558904.
- Benjamin Michaud, François Bailly, Eve Charbonneau, Amedeo Ceglia, Léa Sanchez, and Mickael Begon. Bioptim, a Python framework for Musculoskeletal Optimal Control in Biomechanics. *IEEE Transactions on Systems, Man, and Cybernetics: Systems*, pages 1 – 12, 2022. doi:10.1109/TSMC.2022.3183831.
- K. Wright. Some relationships between implicit Runge-Kutta, collocation and Lanczos $\tau$  methods, and their stability properties. *BIT Numerical Mathematics 1970 10:2*, 10(2):217–227, 6 1970. doi:10.1007/BF01936868.
- Recherche Opérationnelle Série, Rouge A Guillou, and J L Soulé. La résolution numérique des problèmes différentiels aux conditions initiales par des méthodes de collocation. *Revue française d’informatique et de recherche opérationnelle. Série rouge*, 3(R3):17–44, 1969.
- Ernst Hairer, Gerhard Wanner, and Christian Lubich. Numerical Integrators. *Geometric Numerical Integration*, pages 27–50, 5 2006. doi:10.1007/3-540-30666-8\_2.
- Roy Featherstone. Divide-and-conquer articulated-body algorithm for parallel  $O(\log(n))$  calculation of rigid-body dynamics. Part 1: Basic algorithm. *International Journal of Robotics Research*, 18(9):867–875, 1999. doi:10.1177/02783649922066619.
- Roy Featherstone. *Robot Dynamics Algorithms*. Springer New York, NY, 1987. doi:10.1007/978-0-387-74315-8.
- François Bailly, Amedeo Ceglia, Benjamin Michaud, Dominique M. Rouleau, and Mickael Begon. Real-Time and Dynamically Consistent Estimation of Muscle Forces Using a Moving Horizon EMG-Marker Tracking Algorithm—Application to Upper Limb Biomechanics. *Frontiers in Bioengineering and Biotechnology*, 9:112, 2 2021a. doi:10.3389/fbioe.2021.642742.

- Darko Trivun, Haris Dindo, and Bakir Lacevic. Resilient hexapod robot. *ICAT 2017 - 26th International Conference on Information, Communication and Automation Technologies, Proceedings*, 2017-December:1–6, 12 2017. doi:10.1109/ICAT.2017.8171613.
- Wen Wu, Peter V.S. Lee, Adam L. Bryant, Mary Galea, and David C. Ackland. Subject-specific musculoskeletal modeling in the evaluation of shoulder muscle and joint function. *Journal of Biomechanics*, 49(15):3626–3634, 11 2016. doi:10.1016/j.jbiomech.2016.09.025.
- Gil Serrancolí and Rosa Pàmies-Vilà. Analysis of the influence of coordinate and dynamic formulations on solving biomechanical optimal control problems. *Mechanism and Machine Theory*, 142:103578, 12 2019. doi:10.1016/j.mechmachtheory.2019.103578.
- M. R. Yeadon. The simulation of aerial movement—II. A mathematical inertia model of the human body. *Journal of Biomechanics*, 23(1):67–74, 1 1990. doi:10.1016/0021-9290(90)90370-I.
- Pierre Puchaud. `github.com/Ipuch/dms-vs-dc: 0.2.0`, 1 2023.
- Andreas Wächter and Lorenz T. Biegler. On the implementation of an interior-point filter line-search algorithm for large-scale nonlinear programming. *Mathematical Programming*, 106(1):25–57, 2006. doi:10.1007/s10107-004-0559-y.
- Iain S. Duff. MA57 - A code for the solution of sparse symmetric definite and indefinite systems. *ACM Transactions on Mathematical Software*, 30(2):118–144, 2004. doi:10.1145/992200.992202.
- Ernst Hairer and Gerhard Wanner. *Solving Ordinary Differential Equations II*, volume 14 of *Springer Series in Computational Mathematics*. Springer Berlin Heidelberg, Berlin, Heidelberg, 1996. doi:10.1007/978-3-642-05221-7.
- Robin Verschueren, Gianluca Frison, Dimitris Kouzoupis, Jonathan Frey, Niels van Duijkeren, Andrea Zanelli, Branimir Novoselnik, Thivaharan Albin, Rien Quirynen, and Moritz Diehl. `acados`—a modular open-source framework for fast embedded optimal control. *Mathematical Programming Computation*, 14(1):147–183, 3 2022. doi:10.1007/S12532-021-00208-8/TABLES/8.
- Christopher L Dembia, Nicholas A Bianco, Antoine Falisse, Jennifer L Hicks, and Scott L Delp. OpenSim Moco: Musculoskeletal optimal control. *PLoS Computational Biology*, 16(12 December):839381, 11 2020. doi:10.1371/journal.pcbi.1008493.
- François Bailly, Eve Charbonneau, Loane Danès, and Mickael Begon. Optimal 3D arm strategies for maximizing twist rotation during somersault of a rigid-body model. *Multibody System Dynamics*, 52(2):193–209, 6 2021b. doi:10.1007/S11044-020-09759-5/FIGURES/11.
- Anne D. Koelewijn and Antonie J. van den Bogert. A solution method for predictive simulations in a stochastic environment. *Journal of Biomechanics*, 104, 5 2020. doi:10.1016/J.JBIOMECH.2020.109759.
- Míriam Febrer-Nafria, Roger Pallarès-López, Benjamin J. Fregly, and Josep M. Font-Llagunes. Prediction of three-dimensional crutch walking patterns using a torque-driven model. *Multibody System Dynamics*, 51(1):1–19, 2021. doi:10.1007/s11044-020-09751-z.
- Younguk Kim, Yihwan Jung, Woosung Choi, Kunwoo Lee, and Seungbum Koo. Similarities and differences between musculoskeletal simulations of OpenSim and AnyBody modeling system. *Journal of Mechanical Science and Technology*, 32(12):6037–6044, 12 2018. doi:10.1007/s12206-018-1154-0.
- Daniel B. Leineweber, Andreas Schäfer, Hans Georg Bock, and Johannes P. Schlöder. An efficient multiple shooting based reduced SQP strategy for large-scale dynamic process optimization: Part II: Software aspects and applications. *Computers & Chemical Engineering*, 27(2):167–174, 2 2003. doi:10.1016/S0098-1354(02)00195-3.
- Francesco Ruscelli, Arturo Laurenzi, Nikos G. Tsagarakis, and Enrico Mingo Hoffman. Horizon: A Trajectory Optimization Framework for Robotic Systems. *Frontiers in Robotics and AI*, 9:148, 7 2022. doi:10.3389/FROBT.2022.899025/BIBTEX.
- Jonathan Frey, Jochem De Schutter, and Moritz Diehl. Fast integrators with sensitivity propagation for use in CasADi. *arXiv*, 11 2022. doi:10.48550/arxiv.2211.01982.
- Sina Porsa, Yi Chung Lin, and Marcus G. Pandy. Direct Methods for Predicting Movement Biomechanics Based Upon Optimal Control Theory with Implementation in OpenSim. *Annals of biomedical engineering*, 44(8):2542–2557, 8 2016. doi:10.1007/S10439-015-1538-6.
- Alexis D. Gidley, Anthony P. Marsh, and Brian R. Umberger. Performance criteria for generating predictive optimal control simulations of bicycle pedaling. *Computer Methods in Biomechanics and Biomedical Engineering*, 22(1): 11–20, 1 2018. doi:10.1080/10255842.2018.1522535.
- Colin Brown and John McPhee. Predictive forward dynamic simulation of manual wheelchair propulsion on a rolling dynamometer. *Journal of Biomechanical Engineering*, 142(7), 2020. doi:10.1115/1.4046298.

- R Quirynen, S Gros, and M Diehl. Lifted implicit integrators for direct optimal control. In *54th IEEE Conference on Decision and Control (CDC)*, pages 3212–3217, Osaka, Japan, 12 2015. IEEE.
- Elliot R. Johnson and Todd D. Murphey. Scalable variational integrators for constrained mechanical systems in generalized coordinates. *IEEE Transactions on Robotics*, 25(6):1249–1261, 12 2009. doi:10.1109/TRO.2009.2032955.
- Benoit Mariani, Stephane Rochat, Christophe J. Büla, and Kamiar Aminian. Heel and toe clearance estimation for gait analysis using wireless inertial sensors. *IEEE Transactions on Biomedical Engineering*, 59(12 PART2):3162–3168, 2012. doi:10.1109/TBME.2012.2216263.
- Tim W. Dorn, Jack M. Wang, Jennifer L. Hicks, and Scott L. Delp. Predictive Simulation Generates Human Adaptations during Loaded and Inclined Walking. *PLOS ONE*, 10(4):e0121407, 4 2015. doi:10.1371/JOURNAL.PONE.0121407.
- Carmichael F. Ong, Thomas Geijtenbeek, Jennifer L. Hicks, and Scott L. Delp. Predicting gait adaptations due to ankle plantarflexor muscle weakness and contracture using physics-based musculoskeletal simulations. *PLOS Computational Biology*, 15(10):e1006993, 10 2019. doi:10.1371/JOURNAL.PCBI.1006993.
- Vinh Q. Nguyen, Russell T. Johnson, Frank C. Sup, and Brian R. Umberger. Bilevel Optimization for Cost Function Determination in Dynamic Simulation of Human Gait. *IEEE Transactions on Neural Systems and Rehabilitation Engineering*, 27(7):1426–1435, 7 2019. doi:10.1109/TNSRE.2019.2922942.
- K. Veerkamp, N. F.J. Waterval, T. Geijtenbeek, C. P. Carty, D. G. Lloyd, J. Harlaar, and M. M. van der Krogt. Evaluating cost function criteria in predicting healthy gait. *Journal of Biomechanics*, 123:110530, 6 2021. doi:10.1016/J.JBIOMECH.2021.110530.

## A Detailed OCPs

### A.1 Torque-driven robot leg pointing task

**Multibody model.** A three-DoF kinematic chain articulated with three hinges (Fig. 2).

**Task.** The end-effector of the robot is constrained to reach specified locations at  $t_0$  and  $t_f$  with null joint velocities  $\dot{\mathbf{q}}(t_0) = \dot{\mathbf{q}}(t_f) = \mathbf{0}$ . A Lagrange term minimizes joint torques and velocity, leading to the following cost function:

$$\Phi = \omega_1 \int_{t_0}^{t_f} \boldsymbol{\tau}^2 dt + \omega_2 \int_{t_0}^{t_f} \dot{\mathbf{q}}^2 dt \quad (10)$$

with  $\omega_1$  and  $\omega_2$  set to 1 and 1e-6, respectively.

### A.2 Torque-driven 6 DoF pendulum equilibrium

**Multibody model.** The model is a 3D robotic arm with an inverted pendulum attached to its end-effector, adapted from Docquier et al. [2019]. It consists of 4 bodies and 6 DoFs. The first element is connected to the base with two hinges. A hinge joint connects the second and third elements. A universal joint characterizes the pendulum's motion relative to the end-effector.

**Task.** The robot's end-effector is constrained to reach a specified location at  $t_0$  and  $t_f$ . The velocity of the end-effector is also constrained to be zero. In a stable equilibrium, the initial conditions of the system are given by:  $\dot{\mathbf{q}}(t_0) = \mathbf{0}$ , and  $\ddot{\mathbf{q}}(t_0) = \mathbf{0}$ . A terminal constraint ensures the pendulum remains vertical at the final instant  $t_f$ . The following objective is defined:

$$\Phi = \omega_1 \int_{t_0}^{t_f} \boldsymbol{\tau}^2 dt + \omega_2 \int_{t_0}^{t_f} \Delta \boldsymbol{\tau}^2 dt + \omega_3 \int_{t_0}^{t_f} \dot{\mathbf{q}}^2 dt \quad (11)$$

with  $\Delta \boldsymbol{\tau}$ , the rate of change of the torques  $\boldsymbol{\tau}$ . Weights  $\omega_1, \omega_2, \omega_3$ , are set to 1, 1 and 1e-2, respectively.

### A.3 Muscle-driven upper limb pointing task

**Multibody model.** A 5-segment, 10-DoF upper-limb musculoskeletal model from [Wu et al., 2016] is implemented in Biorbd. The forearm and wrist are modeled as rigid-body segments connected to the elbow via a 2-DoF universal joint, and the glenohumeral joint and acromioclavicular joints are modeled as 3-DoF ball-and-socket joints. The sternoclavicular joint is modeled as a 2-DoF joint. Twenty-six muscle units represented the major muscle groups of the axial scapula, axial humerus, and glenohumeral. Residual torques are considered for each DoF except for the glenohumeral joint.

**Task.** The goal is to reach the head from a reference position with zero velocity at the beginning and the end of the task. Reference trajectories  $\mathbf{q}$  are computed using inverse kinematics on experimental data. The reference trajectories bound the initial and final time of the simulation. Joint torques, their rate of change, and muscle forces are minimized. Regularization objectives are set to ease the convergence. Generalized coordinates of the sternoclavicular and acromioclavicular joints are minimized to maintain the scapula as close as possible to its original position. Joint velocities and their rate of change are also minimized. Finally, a Mayer term minimizes the velocity to reach zero velocity at the end. As a result, the cost function was a sum of Lagrange and Mayer terms:

$$\begin{aligned} \mathcal{J} = & \omega_1 \int_{t_0}^{t_f} \boldsymbol{\tau}_{res}^\top \boldsymbol{\tau}_{res} dt + \omega_2 \int_{t_0}^{t_f} \Delta \boldsymbol{\tau}_{res}^\top \Delta \boldsymbol{\tau}_{res} dt \\ & + \omega_3 \sum_{k=0}^4 \int_{t_0}^{t_f} \mathbf{q}_i^\top \mathbf{q}_i dt + \omega_4 \int_{t_0}^{t_f} \dot{\mathbf{q}}^\top \dot{\mathbf{q}} dt + \omega_5 \int_{t_0}^{t_f} \Delta \dot{\mathbf{q}}^\top \Delta \dot{\mathbf{q}} dt \\ & \omega_6 \dot{\mathbf{q}}(t_f)^2, \end{aligned} \quad (12)$$

$$(13)$$

where weights  $\omega_1, \omega_2, \omega_3, \omega_4, \omega_5, \omega_6$  are respectively set to 10, 1500, 1000, 200, 150, and 0.5.

#### A.4 Torque-driven Planar human

**Multibody model.** A 12-DoFs planar human model is implemented as in Serrancolí and Pàmies-Vilà [2019]. The model has three unactuated DoFs at the torso segment to freely move in the global frame. It comprises two hips, two knees, a neck, two shoulders, and two elbow joints. The model is based on a human of 83 kg and 1.67 m in height.

**Task.** The optimal control problem simulates a half-cycle walking gait with constrained dynamics [Felis and Mombaur, 2016]. A constraint is set to ensure the location of the right foot at  $t_0$  and its zero velocity. A constraint that defines a step length of 0.8 m enforces the initial and final location of the left foot. A heel clearance constraint is added to ensure the lifting of the foot between 4 and 6 cm over the floor in the middle of the simulation [Mariani et al., 2012]. Arm swing is also enforced through initial and terminal bounds. The vertical component of the ground reaction force is constrained to be positive. Torque actuators are minimized to accomplish the task. A stability criterion minimizes the floating base and head joint accelerations with a weight of 0.01 as in previous studies [Dorn et al., 2015, Ong et al., 2019, Nguyen et al., 2019, Veerkamp et al., 2021]. Two Mayer cost functions at  $t_0$  and  $t_f$  ensure the constant gait velocity, by tracking the horizontal center of mass velocity at  $\dot{c}_y^{ref} = 1.3 \text{ m/s}$ . As a result, the cost function is a sum of Lagrange and Mayer terms:

$$\begin{aligned} \Phi = & \omega_1 \int_{t_0}^{t_f} \boldsymbol{\tau}_J^\top \boldsymbol{\tau}_J dt + \omega_2 \sum_{k=0}^3 \int_{t_0}^{t_f} \ddot{\mathbf{q}}_k^\top \ddot{\mathbf{q}}_k dt \\ & + \omega_3 \left( (\dot{c}_y(t_0) - \dot{c}_y^{ref})^2 + (\dot{c}_y(t_f) - \dot{c}_y^{ref})^2 \right) \end{aligned} \quad (14)$$

where  $k^{\text{th}}$   $\mathbf{q}$  stands for the four first DoFs.  $t_0$  is the initial instant of time of the OCP. Weight  $\omega_1, \omega_2, \omega_3$ , is respectively set to 1, 0.01, and 1000.

**Equations of motions.** The equations of motion includes an inelastic contact constraint such that:

$$M(\mathbf{q})\ddot{\mathbf{q}} + N(\mathbf{q}, \dot{\mathbf{q}}) = S^\top \boldsymbol{\tau}_J + K(\mathbf{q})^\top \boldsymbol{\lambda} \quad (15)$$

$$K(\mathbf{q})\ddot{\mathbf{q}} + \dot{K}(\mathbf{q})\dot{\mathbf{q}} = \mathbf{0} \quad (16)$$

where  $K(\mathbf{q})$  is the jacobian constraint,  $\boldsymbol{\lambda}$  are the Lagrange multipliers, which correspond to the contact forces. The system can be rewritten to be handled as an ordinary differential equation by writing Eq. (15) and (16) into a linear system of the unknowns  $\ddot{\mathbf{q}}$ , and  $\boldsymbol{\lambda}$ :

$$\begin{bmatrix} M(\mathbf{q}) & K(\mathbf{q})^\top \\ K(\mathbf{q}) & \mathbf{0} \end{bmatrix} \begin{pmatrix} \ddot{\mathbf{q}} \\ \boldsymbol{\lambda} \end{pmatrix} = \begin{pmatrix} -N(\mathbf{q}, \dot{\mathbf{q}}) + S^\top \boldsymbol{\tau}_J \\ -\dot{K}(\mathbf{q})\dot{\mathbf{q}} \end{pmatrix} \quad (17)$$

Consistency conditions ensure the first frame to respect the constraints  $h(\mathbf{q}) = \mathbf{0}$  and  $K(\mathbf{q})\dot{\mathbf{q}} = \mathbf{0}$ . This equation can be re-written as a differential algebraic equation and can be integrated an ODE  $\dot{\mathbf{x}} = f(\mathbf{x}, \mathbf{u})$  as for the classical forward dynamics equation by setting states  $\mathbf{x} = [\mathbf{q}, \dot{\mathbf{q}}]$  and controls  $\mathbf{u} = \boldsymbol{\tau}_J$ .

**Bounds and initial Guess.** The state's boundaries are set to get plausible joint ranges of motion for gait. The torso rotational DoF could only bend forward. The initial and final head joint velocity is constrained at a zero velocity. The initial knee flexions are limited to  $\frac{\pi}{8}$ . To get shoulder oscillations, initial right and left shoulder states are set to  $-\frac{\pi}{6}$  and  $\frac{\pi}{6}$  and reversed for the final states. The initial and final shoulder velocities are set to zero. All torque controls were bounded between -500 and 500 Nm except for the three controls of the torso segment, considered the root segment, which were bounded to zero.

Initial and final poses are computed through inverse kinematics, ensuring right and left feet are at the specified locations, and root segment has positive generalized coordinates to be within boundaries. The initial guess of the generalized coordinates is computed from a linear interpolation from the initial to the final pose. The initial guesses of generalized velocities  $\dot{\mathbf{q}}$  and control torques  $\boldsymbol{\tau}$  is set to zero.

#### A.5 Torque-driven double twisted somersault

**Multibody model.** The human body model includes 15 DoFs [Puchaud et al., 2023]: 6 DoFs for the floating base, 3 for the thoracolumbar joint (flexion, lateral flexion, and axial rotation), 2 for each shoulder (plane of elevation and elevation), and 2 modeling right and left hips (flexion and abduction). The model inertial parameters is based on 95 anthropometric measures of an elite trampolinist (male, 18 years old, 73.6 kg, 170.8 cm), in line with Yeadon's anthropometric model [Yeadon, 1990].

**Task.** The goal is to execute 1 twist in  $1\frac{3}{4}$  of somersaults from takeoff to the prelanding phase. Final time  $t_f$  is an optimized parameter of the OCP, constrained to remain between  $\pm 0.05$  s representative of the performance of an athlete measured in Venne et al. [2022]. The objective function enforces the execution of the twisting somersault while minimizing hands and feet trajectories in pelvis frames. Integral of joint torques  $\tau_j$  are minimized. To ensure smooth joint kinematics, joint torques, and joint velocities rate of change denoted,  $\Delta\tau_J$ ,  $\Delta\dot{q}_J$  are minimized. An objective term includes states of core DoFs, namely thoracolumbar joint and hips, which were denoted  $\mathcal{C}_{dof}$  so that the gymnast stays as straight as possible to comply with the sports regulations. Specific Mayer term  $\mathcal{M}$  is added to minimize angular momentum  $\sigma$  at the initial instant of time  $t_0$ . Finally, the objective function is a sum of terms  $\mathcal{J}$  and  $\mathcal{M}$ :

$$\begin{aligned} \mathcal{J} = & \omega_1 \sum_{k=1}^3 \left( \Delta \underline{P}^k \right)^2 + \omega_2 \int_{t_0}^{t_f} \tau_J^\top \tau_J dt \\ & + \omega_2 \int_{t_0}^{t_f} \Delta \tau_J^\top \Delta \tau_J dt + \omega_3 \int_{t_0}^{t_f} \Delta \dot{q}_J^\top \Delta \dot{q}_J dt \\ & + \omega_4 \sum_{k \in \mathcal{C}_{dof}} \int_{t_0}^{t_f} q_k^2 dt + \omega_5 t_f \end{aligned} \quad (18)$$

$$\mathcal{M} = \omega_6 \sigma_x(t_0) + \omega_6 (\sigma_y(t_0)^2 + \sigma_z(t_0)^2) \quad (19)$$

where  $\Delta \underline{P}^k$  is  $k^{\text{th}}$  rate of change of path of hands ( $k = 1, 2$ ) or foot ( $k = 3$ ) in pelvis frame for each instant of time of the problem,  $t_0$  is the initial instant of time of the OCP. Weight  $\omega_1, \omega_2, \omega_3, \omega_4, \omega_5, \omega_6$  are set to 10, 100, 100, 10,  $10^{-6}$  and 50, respectively.

## B Noise applied to initial guesses of OCP

Table 1: Noise magnitude applied on decision variables for each OCP in percentage (%) of bound magnitude

<b>OCP</b>	<b>1</b>	<b>2</b>	<b>3</b>	<b>4</b>	<b>5</b>
<b>Model</b>	Leg	Arm	Acrobat	Planar human	Upper limb
$q_{\text{init}}$	zeros	zeros	custom	linear	linear
$\dot{q}_{\text{init}}$	zeros	zeros	custom	zeros	zeros
$\tau_{\text{init}}$	zeros	zeros	custom	zeros	zeros
$a_{\text{init}}$	-	-	-	-	constant
Noise magnitude (%)					
$q$	100	50	20 - 56	10	1
$\dot{q}$	100	50	2	1	0.2
$\tau$	20	50	2	1	1
$a$	-	-	-	-	2

Notes: All the noise magnitudes were chosen to keep the initial guess within the bounds of the decision variables.